Structural Engineering and Mechanics, *Vol. 61, No. 4 (2017) 497-510*
DOI: https://doi.org/10.12989/sem.2017.61.4.497

Auto-parametric resonance of framed structures under periodic excitations

Yuchun Li*, Hongliang Gou[a], Long Zhang[b] and Chenyu Chang[c]

Department of Hydraulic Engineering, College of Civil Engineering, Tongji University, Shanghai, China

(Received July 17, 2016, Revised October 19, 2016, Accepted November 18, 2016)

Abstract. A framed structure may be composed of two sub-structures, which are linked by a hinged joint. One sub-structure is the primary system and the other is the secondary system. The primary system, which is subjected to the periodic external load, can give rise to an auto-parametric resonance of the second system. Considering the geometric-stiffness effect produced by the axially internal force, the element equation of motion is derived by the extended Hamilton's principle. The element equations are then assembled into the global non-homogeneous Mathieu-Hill equations. The Newmark's method is introduced to solve the time-history responses of the non-homogeneous Mathieu-Hill equations. The energy-growth exponent/coefficient (EGE/EGC) and a finite-time Lyapunov exponent (FLE) are proposed for determining the auto-parametric instability boundaries of the structural system. The auto-parametric instabilities are numerically analyzed for the two frames. The influence of relative stiffness between the primary and secondary systems on the auto-parametric instability boundaries is investigated. A phenomenon of the "auto-parametric internal resonance" (the auto-parametric resonance of the second system induced by a normal resonance of the primary system) is predicted through the two numerical examples. The risk of auto-parametric internal resonance is emphasized. An auto-parametric resonance experiment of a Γ-shaped frame is conducted for verifying the theoretical predictions and present calculation method.

Keywords: auto-parametric resonance; framed structures; finite element modeling; non-homogeneous Mathieu-Hill equation; energy-growth exponent/coefficient (EGE/EGC);finite-time Lyapunov exponent (FLE); experiment

1. Introduction

The engineering structures are often subjected to periodic loads. For examples, a rotating machine system is usually exerted a periodic unbalanced inertia force, a bridge is frequently subjected to the cyclical loads from the running vehicles, a marine structure is always suffered the periodic wave forces etc. When the frequency of excitation has a certain quantity relation with the natural frequency of the structure, the structural system may undergo a resonance. Generally, the normal resonance, in which the forcing frequency coincides with the natural frequency of the structure, is highly focused by the structural designers. Meanwhile the principle parametric (or auto-parametric) resonance, in which the excitation frequency is twice the natural frequency of the structure (or sub-structure), is a secondary interest, however it can have a catastrophic effect on structures near the critical regions of parametric (or auto-parametric) instability.

On the basis of the analytical methods, the parametric vibration (dynamic stability) problems of a single-span beam with different constrains have been well investigated and documented by Bolotin (1964), Majorana and Pellegrino (1997), Majorana and Pomaro (2011, 2012), Xie (2006).

With the aid of the finite element method (FEM), Shastry and Rao (1984, 1986) studied dynamic stability of bars considering shear deformation and rotator inertia, and dynamic stability of short cantilever columns subjected to distributed loads. Briseghella *et al*. (1998) analyzed the dynamic stability of beam structures. Basar *et al*. (1987) investigated the parametric resonance phenomena (dynamic instability) of arbitrary elastic shell structures. Pradyumna and Gupta (2011) studied the dynamic stability of laminated composite plates with piezoelectric layers. Mishra and Sahu (2015) investigated parametric instability of beams with transverse cracks. Kumar *et al*. (2015) analyzed the parametric resonance (dynamic stability) of composite skew plate under non-uniform in-plane loading. All the above dynamic stability problems of the structures can be described by the following homogeneous Mathieu-Hill equations

$$\mathbf{M}\ddot{\mathbf{a}}(t)+\mathbf{C}\dot{\mathbf{a}}(t)+\left[\mathbf{K}_0-(P_s+P_d\cos\omega t)\cdot\mathbf{K}_g\right]\mathbf{a}(t)=0 \quad (1)$$

where t is the time, $\mathbf{M}$, $\mathbf{C}$, $\mathbf{K}_0$ and $\mathbf{K}_g$ are the (constant) mass, damping, stiffness and geometric stiffness matrices, respectively, $\mathbf{a}(t)$, $\dot{\mathbf{a}}(t)$ and $\ddot{\mathbf{a}}(t)$ are the nodal displacement, velocity and acceleration vectors, respectively, $(P_s+P_d\cos\omega t)$ is an external force that axially exerts on the structure (or component), in which P_s is the static force,

*Corresponding author, Professor
E-mail: YCL2000@tongji.edu.cn
[a]Ph.D. Student
E-mail: 741878698@qq.com
[b]Graduate Student
E-mail: 1232392zhanglong@tongji.edu.cn
[c]Graduate Student
E-mail: changchenyu@163.com

ISSN: 1225-4568 (Print), 1598-6217 (Online)

and P_d and ω are the amplitude and frequency of the dynamic force, respectively. The stability boundaries of Eq. (1) can be determined by the approach proposed by Bolotin (1964). In this method, the displacement vector $\mathbf{a}(t)$ is expanded as the Fourier series with periods T and $2T$, where $T=2\pi/\omega$, and thus the equations that the stability boundary points satisfy are derived. This method has been successfully used in the above references for solving the stability boundaries of the different structures.

The above problems described by Eq. (1) are focused on the dynamic stability of a single-span beam, or a plate, or a shell, or a simple frame, which is directly subjected an axial periodic external force. These problems are called parametric vibrations of structures. However there is also a kind of so-called auto-parametric vibration (resonance) problem in the mechanical and structural systems. Tondl *et al*. (2000) discussed the auto-parametric resonance of mechanical systems in details. When a structural (or mechanical) system consists of two subsystems, one is the primary system and the other is the secondary system. The secondary system is coupled with the primary system in a nonlinear way. The primary system is subjected to the external excitation, and the vibration of the primary system acts as a parametric excitation of the secondary system. The parametric vibration of the secondary system, which is induced by the primary system, is called auto-parametric resonance. Xia and Fujino (2006) investigated the auto-parametric vibration of a cable-stayed-beam system. Recently, Náprstek and Fischer (2015) studied auto-parametric resonance of a vertically excited nonlinear continuous system.

A framed structure is composed of several beams. These beam elements may be linked by hinged joints. If a periodical external force acts on one beam, which is regarded as the primary system, the dynamic load of the primary system can be transmitted into the other beam (i.e., the secondary system) via a hinged joint, and may give rise to the auto-parametric resonance (instability) of the secondary system. It should be emphasized that the dynamic load that directly cause the instability is the transmitted internal axial force, instead of the external load. When the geometric stiffness effects of the internal axial force for each beam are considered, the motion equations of the framed structure can be generally expressed as the following non-homogeneous Mathieu-Hill equation

$$\mathbf{M}\ddot{\mathbf{a}}(t)+\mathbf{C}\dot{\mathbf{a}}(t)+\left[\mathbf{K}-\mathbf{K}_G(t)\right]\mathbf{a}(t)=\mathbf{f}(t) \tag{2}$$

where $\mathbf{f}$(t) is the external force vector, $\mathbf{K}$ is the constant stiffness matrix, $\mathbf{K}_G(t)$ is a time-variable geometric stiffness matrix which directly depends on the internal axial force, or indirectly depends on the $\mathbf{f}(t)$. The auto-parametric instability motion of the framed structure can be simulated by Eq. (2). It should be mentioned that the current commercial codes cannot be directly applied for analyzing the auto-parametric resonances of the framed structures described by Eq. (2). Because the influence of internal (periodic) axial force on the stiffness matrix of beam element is not considered in these codes, the phenomenon of auto-parametric instability of the framed structures cannot be simulated. The investigations about the auto-parametric instability of framed structures related to the non-homogeneous Mathieu-Hill Equation (2) have not been found in the existing literature.

In the unstable regions, if the exciting frequency is denoted as ω, then there are three kinds of parametric (auto-parametric) resonance patterns, i.e., the (1/2) sub-harmonic (in which the system response frequency is $\omega/2$), the harmonic (response frequency ω), and the super-harmonic (the response frequencies are $3\omega/2$, 2ω and $5\omega/2$ etc.). The sub-harmonic response is also called the principal parametric resonance. It has been found from the existing studies (Li and Wang 2016, Li *et al*. 2016) that the principal parametric resonance has an overwhelming advantage among the three unstable patterns. The existing experimental observations of parametric vibrations indicated that the stability consideration can make the occurrence of harmonic and super-harmonic vibrations very difficult. The principal parametric resonance is the most easily-occurred and dangerous resonance pattern. As far as the engineering application is concerned, the principal parametric (or auto-parametric) resonance is exclusively considered in this study.

In this paper, the geometric-stiffness matrix of element, which is produced by the internal axial force, is considered in finite element modeling. The time-history response-based methods are proposed to solve the instability boundaries of auto-parametric resonances. An auto-parametric vibration experiment is conducted to verify the theoretical results. The main purpose of this paper is to provide a practical method for the structural engineers to analyze the auto-parametric resonances of framed structures, and to reveal some potential risks of the auto-parametric resonances.

2. Finite element modeling for parametric and auto-parametric vibrations

2.1 Beam element equation considering geometric stiffness effect of internal axial force

For a structural system, the extended Hamilton's principle is presented as (Clough and Penzien 2003)

$$\delta\int_{t_1}^{t_2} L\cdot dt+\int_{t_1}^{t_2}\sum_{j=1}^{n} Q_j^*\cdot\delta q_j\cdot dt=0 \tag{3}$$

where $L=T-V$ is the Lagrangian, T and V are the kinetic and potential energies of the structural system, respectively, Q_j^* is the non-conservative force, δq_j is the virtual displacement of generalized coordinate, and $\sum_{j=1}^{n} Q_j^*\cdot\delta q_j$ represents the sum of virtual works of all the non-conservative forces. According to (Clough and Penzien 2003), the Hamilton's principle Eq. (3) is valid for any complicated system, linear or nonlinear. The application of this principle leads directly to the equations of motion for any given system.

Consider a uniform beam element in x-y plane shown in Fig. 1, in which the initial length of beam is l, the cross-sectional area A, the line mass density $\bar{m}$, and the flexural rigidity of beam EI. For nodes i and j, the coordinates are

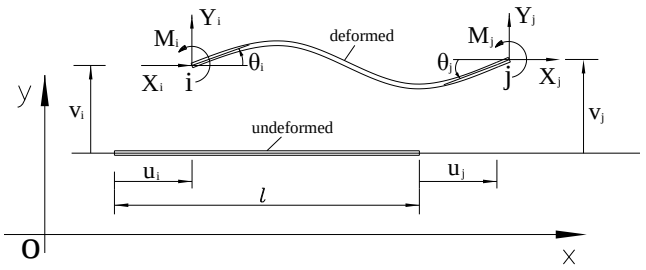

Fig. 1 A uniform beam element

respectively (x_i,y_i) and(x_j,y_j), the nodal forces $\{X_i,Y_i,M_i\}^T$ and $\{X_j,Y_j,M_j\}^T$, and the nodal displacements $\{u_i,v_i,\theta_i\}^T$ and$\{u_j,v_j,\theta_j\}^T$. The kinetic energy of the beam (Bernoulli-Euler beam) can be expressed as

$$T=\frac{1}{2}\int_0^l \bar{m}(\dot{u}^2+\dot{v}^2)dx \tag{4}$$

and the potential energy

$$V=\frac{1}{2}\int_0^l EI(v'')^2dx+\frac{1}{2}\int_0^l EA(u')^2dx \tag{5}$$

where dots and apostrophes respectively refer to differentiations with respect to time t and coordinate x, and u and v are respectively the horizontal and vertical displacements of beam element.

The axial shortness of the beam due to the bending deformation is

$$\Delta=\frac{1}{2}\int_0^l (v')^2dx \tag{6}$$

The virtual work by the nodal (non-conservative) forces on the corresponding virtual displacements can be written as

$$\sum_{j=1}^{n} Q_j^*\cdot\delta q_j=\delta\mathbf{a}_\mathbf{e}^T(t)\cdot\mathbf{r}_\mathbf{e}(t)+\frac{1}{2}(X_i-X_j)\cdot\delta\Delta \tag{7}$$

where

$$\begin{cases}\mathbf{r}_\mathbf{e}^T(t)=\{X_i,Y_i,M_i,X_j,Y_j,M_j\}^T\\ \mathbf{a}_\mathbf{e}^T(t)=\{u_i,v_i,\theta_i,u_j,v_j,\theta_j\}^T\end{cases} \tag{8}$$

in which $\mathbf{r}_\mathbf{e}(t)$ and $\mathbf{a}_\mathbf{e}(t)$ are respectively the nodal force and displacement vectors of beam element. The first term of Eq. (7) represents the virtual work of nodal forces, and the second term is just the virtual work by the internal axial forces (X_i, X_j) on the virtual displacement $\delta\Delta$. The second term of Eq. (7) is generally neglected in finite element modeling when the dynamic instability of the beam is not considered. However, this term plays a crucial role in the parametric (or auto-parametric) resonance. It is the second term that arouses the dynamic instability of structure. Therefore the second term must be considered in the analyses of dynamic stability. The displacements of beam element can be assumed as (Wang 2003, Bathe 1996)

$$\begin{cases}u=\mathbf{N}_u^T\mathbf{a}_\mathbf{e}(t)\\ v=\mathbf{N}_v^T\mathbf{a}_\mathbf{e}(t)\end{cases} \tag{9}$$

where $\mathbf{N}_u^T$ and $\mathbf{N}_v^T$ are respectively the vectors of shape functions, which are expressed as

$$\begin{cases}\mathbf{N}_u^T=\{N_{u1},0,0,N_{u2},0,0\}^T\\ \mathbf{N}_v^T=\{0,N_{v1},N_{v2},0,N_{v3},N_{v4}\}^T\end{cases} \tag{10}$$

in which

$$\begin{cases}N_{u1}=\frac{1}{2}\left[1-\frac{2}{l}\left(x-\frac{x_i+x_j}{2}\right)\right]\\ N_{u2}=\frac{1}{2}\left[1+\frac{2}{l}\left(x-\frac{x_i+x_j}{2}\right)\right]\\ N_{v1}=1-3\xi^2+2\xi^3\\ N_{v2}=(\xi-2\xi^2+\xi^3)l\\ N_{v3}=3\xi^2-2\xi^3\\ N_{v4}=(\xi^3-\xi^2)l\end{cases} \tag{11}$$

and

$$\xi=\frac{x-x_i}{l} \tag{12}$$

The variable ξ is the dimensionless coordinate of the shape function. Substituting Eqs. (4), (5) and (7) into Eq. (3), employing Eq. (6) and Eqs. (8)-(12), and doing a variational operation, we can obtain the motion equation of beam element

$$\mathbf{M}_\mathbf{e}\ddot{\mathbf{a}}_\mathbf{e}(t)+\mathbf{K}_\mathbf{e}\mathbf{a}_\mathbf{e}(t)-\frac{1}{2}(X_i-X_j)\mathbf{K}_\mathbf{Ge}\mathbf{a}_\mathbf{e}(t)=\mathbf{r}_\mathbf{e}(t) \tag{13}$$

where

$$\mathbf{M}_\mathbf{e}=\bar{m}\int_0^l \mathbf{N}_u\mathbf{N}_u^Tdx+\bar{m}\int_0^l \mathbf{N}_v\mathbf{N}_v^Tdx$$

$$=\frac{\bar{m}l}{630}\begin{bmatrix}210&0&0&105&0&0\\0&234&33l&0&81&-19.5l\\0&33l&6l^2&0&19.5l&-4.5l^2\\105&0&0&210&0&0\\0&81&19.5l&0&234&-33l\\0&-19.5l&-4.5l^2&0&-33l&6l^2\end{bmatrix} \tag{14}$$

$$\mathbf{K}_\mathbf{e}=EA\int_0^l \mathbf{N}_u'\mathbf{N}_u'^Tdx+EI\int_0^l \mathbf{N}_v''\mathbf{N}_v''^Tdx$$

$$=\begin{bmatrix}\frac{EA}{l}&0&0&-\frac{EA}{l}&0&0\\0&\frac{12EI}{l^3}&\frac{6EI}{l^2}&0&-\frac{12EI}{l^3}&\frac{6EI}{l^2}\\0&\frac{6EI}{l^2}&\frac{4EI}{l}&0&-\frac{6EI}{l^2}&\frac{2EI}{l}\\-\frac{EA}{l}&0&0&\frac{EA}{l}&0&0\\0&-\frac{12EI}{l^3}&-\frac{6EI}{l^2}&0&\frac{12EI}{l^3}&-\frac{6EI}{l^2}\\0&\frac{6EI}{l^2}&\frac{2EI}{l}&0&-\frac{6EI}{l^2}&\frac{4EI}{l}\end{bmatrix} \tag{15}$$

$$\mathbf{K}_{\mathbf{Ge}} = \int_0^l \mathbf{N}_v' \mathbf{N}_v'^T dx$$

$$= \begin{bmatrix} 0 & 0 & 0 & 0 & 0 & 0 \\ 0 & \frac{6}{5l} & \frac{1}{10} & 0 & -\frac{6}{5l} & \frac{1}{10} \\ 0 & \frac{1}{10} & \frac{2}{15}l & 0 & -\frac{1}{10} & -\frac{1}{30}l \\ 0 & 0 & 0 & 0 & 0 & 0 \\ 0 & -\frac{6}{5l} & -\frac{1}{10} & 0 & \frac{6}{5l} & -\frac{1}{10} \\ 0 & \frac{1}{10} & -\frac{1}{30}l & 0 & -\frac{1}{10} & \frac{2}{15}l \end{bmatrix} \tag{16}$$

Eq. (13) is rewritten as

$$\mathbf{M_e}\ddot{\mathbf{a}}_\mathbf{e}(t) + \left[\mathbf{K_e} - f_e(t)\cdot\mathbf{K_{Ge}}\right]\mathbf{a_e}(t) = \mathbf{r_e}(t) \tag{17}$$

where

$$\begin{cases} f_e(t) = \boldsymbol{\alpha}^T \mathbf{r_e}(t) \\ \boldsymbol{\alpha}^T = (1/2, 0, 0, -1/2, 0, 0) \end{cases} \tag{18}$$

in which $\mathbf{M_e}$ and $\mathbf{K_e}$ are respectively the element mass and stiffness matrices, $\ddot{\mathbf{a}}_\mathbf{e}(t)$ the element nodal acceleration vector, $f_e(t)\cdot\mathbf{K_{Ge}}$ the element geometric stiffness matrix, in which $f_e(t)$ is the average axially compressive force of beam element. By means of Eqs. (17) and (18), $f_e(t)$ can be further expressed as

$$f_e(t) = \boldsymbol{\alpha}^T \left[\mathbf{I} + \mathbf{K_{Ge}}\mathbf{a_e}(t)\boldsymbol{\alpha}^T\right]^{-1}\left[\mathbf{M_e}\ddot{\mathbf{a}}_\mathbf{e}(t) + \mathbf{K_e}\mathbf{a_e}(t)\right] \tag{19}$$

where $\mathbf{I}$ is the unit matrix. When the nodal displacement and acceleration vectors are known, the axial force $f_e(t)$ can be calculated with Eq. (19).

It can be easily found that the standard shape functions of beam element are introduced in the above finite element formulation. However an additional geometric stiffness matrix is considered in the present formulation.

2.2 The global finite element motion equations of framed structures

If the element geometric stiffness matrix is considered for all the beam elements (or partial elements) of the framed structures, all element matrices can be assembled to the global motion equations as follows

$$\mathbf{M}\ddot{\mathbf{a}}(t) + \mathbf{C}\dot{\mathbf{a}}(t) + \left[\mathbf{K} - \mathbf{K_G}(t)\right]\mathbf{a}(t) = \mathbf{p}(t) \tag{20}$$

where $\mathbf{M}$, $\mathbf{C}$ and $\mathbf{K}$ are respectively the global mass, damping and stiffness matrices; $\ddot{\mathbf{a}}(t)$, $\dot{\mathbf{a}}(t)$ and $\mathbf{a}(t)$ are respectively the global nodal acceleration, velocity and displacement vectors; $\mathbf{p}(t)$ is the global (external) load vector; $\mathbf{K_G}(t)$ is the global geometric stiffness matrix which can be expressed as

$$\mathbf{K_G}(t) = \sum_{e=1}^{n_1} f_e(t)\tilde{\mathbf{K}}_{\mathbf{G}e} \tag{21}$$

where e denotes the element number, n_1 is the total number of the elements, in which the effects of internal axial force are considered, and $f_e(t)\cdot\tilde{\mathbf{K}}_{\mathbf{G}e}$ is the expanded element geometric stiffness matrix. For every time step, each element geometric stiffness matrix will be updated and assembled to the global matrix as time progresses. The damping $\mathbf{C}$ can be constructed separately. Generally speaking, the mechanism of structural damping is very complicated, the damping term $\mathbf{C}\dot{\mathbf{a}}(t)$ cannot be directly obtained from Eq. (3) using the usual operations. In the theory of structural dynamics (Clough and Penzien 2003; Chopra 2007), the damping matrix can be obtained through a Rayleigh damping $\mathbf{C}=\beta_k\mathbf{K}+\beta_m\mathrm{M}$, where the coefficients β_k and β_m can be determined by the modal frequencies and damping ratios.

It should be noted that the geometric stiffness matrix is generally produced by the static and dynamic parts of the internal axial load. The effect of the static part, which only changes the natural frequencies of the structural system, can be absorbed in the constant stiffness $\mathbf{K}$. The variation of natural frequency only makes the stability boundary curves move horizontally, which is a secondary interest in this study. Only the dynamic part can determine the dynamic instability of the structure. For a clear and concise presentation, the geometric stiffness matrix by the dynamic part of the external load is exclusively considered in the following text.

Eq. (20) is a non-homogeneous Mathieu-Hill equation in the form of matrix. It is difficult to solve the instability problem of Eq. (20) by using the existing methods (such as Bolotin's method, multiple scales method etc.).

2.3 Time-history response solution using Newmark's method

The Newmark's method is employed to solve Eq. (20). The nodal displacement, velocity and acceleration vectors are respectively denoted at two successive time instants t_0 and $t=t_0+\Delta t$ by $\mathbf{a}_0$, $\dot{\mathbf{a}}_0$, $\ddot{\mathbf{a}}_0$ and $\mathbf{a(t)}$, $\dot{\mathbf{a}}\mathbf{(t)}$, $\ddot{\mathbf{a}}\mathbf{(t)}$, where Δt is the time increment. Then the Newmark's time-stepping scheme (Chopra 2007) is presented as follows

$$\begin{cases} \mathbf{a}(t) = \mathbf{a}_0 + \Delta\mathbf{a} \\ \dot{\mathbf{a}}(t) = \frac{2}{\Delta t}\Delta\mathbf{a} - \dot{\mathbf{a}}_0 \\ \ddot{\mathbf{a}}(t) = \frac{4}{\Delta t^2}\Delta\mathbf{a} - \frac{4}{\Delta t}\dot{\mathbf{a}}_0 - \ddot{\mathbf{a}}_0 \end{cases} \tag{22}$$

Substituting Eq. (22) into Eq. (20) yields

$$\tilde{\mathbf{A}}\cdot\Delta a = \tilde{\mathbf{P}} \tag{23}$$

where

$$\begin{cases} \tilde{\mathbf{A}} = \frac{4}{\Delta t^2}\mathbf{M} + \frac{2}{\Delta t}\mathbf{C} + \mathbf{K} - \mathbf{K_G}(t_0 + \Delta t) \\ \tilde{\mathbf{p}} = \tilde{\mathbf{p}}(t_0 + \Delta t) + \frac{4}{\Delta t}\mathbf{M}\dot{\mathbf{a}}_0 + \mathbf{M}\ddot{\mathbf{a}}_0 + \mathbf{C}\dot{\mathbf{a}}_0 - \left[\mathbf{K} - \mathbf{K_G}(t_0 + \Delta t)\right]\mathbf{a}_0 \end{cases} \tag{24}$$

It is noted that the geometric stiffness matrix $\mathbf{K_G}(t_0+\Delta t)$

in Eq. (24) is related to the element axial forces $f_e(t_o+\Delta t)$ (e=1,2,3,…,n_1), which are unknown at time $t=t_o+\Delta t$. In the present formulation, the axial forces $f_e(t_o+\Delta t)$ are approximately replaced by their values at time t_0, i.e., $\mathbf{K_G}(t_0+\Delta t)\approx\mathbf{K_G}(t_0)$, therefore Eq. (24) becomes

$$\begin{cases}\tilde{\mathbf{A}}=\dfrac{4}{\Delta t^2}\mathbf{M}+\dfrac{2}{\Delta t}\mathbf{C}+\mathbf{K}-\mathbf{K_G}(t_0)\\ \tilde{\mathbf{p}}=\tilde{\mathbf{p}}(t_0+\Delta t)+\dfrac{4}{\Delta t}\mathbf{M}\dot{\mathbf{a}}_0+\mathbf{M}\ddot{\mathbf{a}}_0+\mathbf{C}\dot{\mathbf{a}}_0-\left[\mathbf{K}-\mathbf{K_G}(t_0)\right]\mathbf{a}_0\end{cases} \tag{25}$$

Thus the displacement increment $\Delta\mathbf{a}$ can be obtained from the solution of Eqs. (25) and (23). Then the nodal displacement, velocity and acceleration vectors at time $t=t_o+\Delta t$ are calculated by substituting $\Delta\mathbf{a}$ into Eq. (22). Consequently, the dynamic time-history responses of the structure are acquired.

2.4 Time-history response solutions under the displacement excitations

Sect.2.3 is about the response solution of Eq. (20) under the load excitations. For the practical engineering structures (or structural tests), it is sometimes difficult to measure the exciting loads, however it is much easier to measure the structural displacements. If only the displacement excitations are known, the time-history responses of structures can be solved by the following approach.

A simple case is considered here. The structure is assumed to be subjected to a known displacement excitation on the n^{th} DOF (degree of freedom), i.e., the exciting displacement $a_n(t)$, velocity $\dot{a}_n(t)$ and acceleration $\ddot{a}_n(t)$ are known, but the corresponding exciting force $p_n(t)$ is unknown. Then Eq. (20) can be rewritten in the form of block matrix

$$\begin{bmatrix}\mathbf{M}_{n-1} & \mathbf{m}_{n-1}\\ \mathbf{m}_{n-1}^T & m_{nn}\end{bmatrix}\begin{bmatrix}\ddot{\mathbf{a}}_{n-1}(t)\\ \ddot{a}_n(t)\end{bmatrix}+\begin{bmatrix}\mathbf{C}_{n-1} & \mathbf{c}_{n-1}\\ \mathbf{c}_{n-1}^T & c_{nn}\end{bmatrix}\begin{bmatrix}\dot{\mathbf{a}}_{n-1}(t)\\ \dot{a}_n(t)\end{bmatrix}+\begin{bmatrix}\mathbf{K}_{n-1} & \mathbf{k}_{n-1}\\ \mathbf{k}_{n-1}^T & k_{nn}\end{bmatrix}\begin{bmatrix}\mathbf{a}_{n-1}(t)\\ a_n(t)\end{bmatrix}-\begin{bmatrix}\mathbf{K}_{\mathbf{G}n-1} & \mathbf{k}_{\mathbf{G}n-1}\\ \mathbf{k}_{\mathbf{G}n-1}^T & k_{Gnn}\end{bmatrix}\begin{bmatrix}\mathbf{a}_{n-1}(t)\\ a_n(t)\end{bmatrix}=\begin{bmatrix}\mathbf{0}\\ p_n(t)\end{bmatrix} \tag{26}$$

Eq. (26) can be expanded into the following two equations

$$\mathbf{M}_{n-1}\ddot{\mathbf{a}}_{n-1}(t)+\mathbf{C}_{n-1}\dot{\mathbf{a}}_{n-1}(t)+(\mathbf{K}_{n-1}-\mathbf{K}_{\mathbf{G}_{n-1}})\mathbf{a}_{n-1}(t)=\mathbf{p}_{n-1}(t) \tag{27}$$

$$\begin{aligned}p_n(t)=&\mathbf{m}_{n-1}^T\ddot{\mathbf{a}}_{n-1}(t)+\mathbf{c}_{n-1}^T\dot{\mathbf{a}}_{n-1}(t)+(\mathbf{k}_{n-1}^T-\mathbf{k}_{\mathbf{G}n-1}^T)\mathbf{a}_{n-1}(t)\\&+m_{nn}\ddot{a}_n(t)+c_{nn}\dot{a}_n(t)+(k_{nn}-k_{Gnn})a_n(t)\end{aligned} \tag{28}$$

where $\mathbf{p}_{n-1}(t)=-\mathbf{m}_{n-1}\ddot{a}_n(t)-c_{n-1}\dot{a}_n(t)-(\mathbf{k}_{n-1}-\mathbf{k}_{\mathbf{G}n-1})a_n(t)$ is a known excitation vector. Eq. (27) can be solved by the Newmark's formulation as described in Sect.2.3. Introducing the solutions $\ddot{\mathbf{a}}_{n-1}(t)$, $\dot{\mathbf{a}}_{n-1}(t)$ and $\mathbf{a}_{n-1}(t)$ into Eq. (28), we can obtain the exciting force $p_n(t)$.

For the cases of multi-displacement excitations, the response solutions can be resolved by the similar method without any substantial difficulty.

3. Methods for dynamic stability analyses

3.1 Bolotin's method

In some special cases, when an external periodic load $P_d\cos\omega t$ acts on the joint of the framed structure, for instance, the case (Fig. 4(a)) of Sect.4.1.1, the finite element equation Eq. (20) of the framed structure can be reduced to the following homogeneous equation

$$\mathbf{M}\ddot{\mathbf{a}}(t)+\mathbf{C}\dot{\mathbf{a}}(t)+(\mathbf{K}-P_d\cos\omega t\cdot\mathbf{K}_g)\mathbf{a}(t)=0 \tag{29}$$

where $\mathbf{K}_g$ is a constant geometric stiffness matrix. The parametric instability of the structural system is directly aroused by the external load $P_d\cos\omega t$. The problem of auto-parametric vibration is reduced to that of parametric vibration. When the damping is neglected, according to the method proposed by Bolotin (1964) the principal instability boundaries of Eq. (29) can be approximately obtained by the following equations (Basar *et al*. 1987, Briseghella *et al*. 1998)

$$\begin{cases}\left|\mathbf{K}-\dfrac{P_d}{2}\mathbf{K_g}-\dfrac{1}{4}\omega^2\mathbf{M}\right|=0\\ \left|\mathbf{K}+\dfrac{P_d}{2}\mathbf{K_g}-\dfrac{1}{4}\omega^2\mathbf{M}\right|=0\end{cases} \tag{30}$$

The solutions of Eq. (30) deliver two critical values of the excitation frequencies for each load level P_d, and determine the lower and upper boundary curves of the principal instability region.

3.2 The method by using the energy-growth exponent/coefficient

Recently, Li *et al*. (2016) have proposed an energy-growth exponent (EGE) and the corresponding energy-growth coefficient (EGC) for analyzing the stability of parametrically excited systems that are governed by Mathieu equation. In this study, we introduce EGE/EGC to investigate the auto-parametric resonance of framed structures. The instantaneous energy function of the global (or the secondary) structure system can be written as

$$E(t)=\frac{1}{2}\dot{\mathbf{a}}^T(t)\cdot\mathbf{M}\cdot\dot{\mathbf{a}}(t)+\frac{1}{2}\mathbf{a}^T(t)\cdot\left[\mathbf{K}-\mathbf{K_G}(t)\right]\cdot\mathbf{a}(t) \tag{31}$$

The numerical results of present study have showed that when the parametric (or auto-parametric) resonance occurs, the energy of the global (or the secondary) system increases with the time in the overall time-domain. If the initial energy is denoted as $E(t)|_{t=0}=E_0$, then a typical time-history response of the energy function $\ln[E(t)/E_0]$ of the second (structure) system is plotted in Fig. 2. It can be seen that the time-history trajectory appears as a backbone curve superimposed on a small periodic perturbation. The backbone curve of the function $\ln[E(t)/E_0]$ shows an interval of the initial transient disturbance in the initial period of time ($0\le t\le t_1$), and a linear growth after the time t_1 ($t_1<t<t_2$), during which the response amplitude of the structural system is still within the linear limitation. In the linear-growth stage, the energy ratio $E(t)/E_0$ grows approximately in an exponential manner, the growth exponent λ can be approximately evaluated by the slope of backbone curve, i.e.

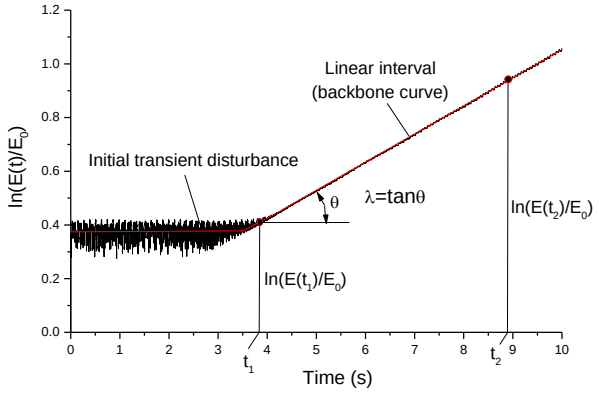

Fig. 2 A typical energy-growth curve of the second (structure) system

$$\lambda = \tan\theta = \frac{1}{t_2 - t_1}\left[\ln\frac{E(t_2)}{E_0} - \ln\frac{E(t_1)}{E_0}\right] = \frac{1}{t_2 - t_1}\ln\frac{E(t_2)}{E(t_1)} \quad (32)$$

The parameter λ in Eq. (32) is defined as the energy-growth exponent (EGE) of unstable motion of the structural system. The EGE, which is independent of the initial conditions (disturbances) of the structural system, represents energy growth speed of the system during the unstable process. The stability of the global (or the second) system can be determined by the following criterion (Li *et al*. 2016)

$$\lambda = \begin{cases} \dfrac{1}{t_2 - t_1}\ln\dfrac{E(t_2)}{E(t_1)} < 0 & \textit{stability} \\ \dfrac{1}{t_2 - t_1}\ln\dfrac{E(t_2)}{E(t_1)} = 0 & \textit{stability boundary} \\ \dfrac{1}{t_2 - t_1}\ln\dfrac{E(t_2)}{E(t_1)} > 0 & \textit{instability} \end{cases} \quad (33)$$

When the global (or the second) system resonates in the j^{th} mode, the corresponding natural frequency is ω_j, then EGE can also be expressed as

$$\lambda_j = \eta_j \omega_j \quad (34)$$

where η_j is a non-dimensional energy-growth coefficient (EGC), which reflects the unstable feature of the parametrically excited system. The EGE and EGC can be numerically determined by Eqs. (20), (31), (32), (33) and (34).

3.3 The method by using the finite-time Lyapunov exponent

3.3.1 The Lyapunov exponent

Xia and Fujino (2006) applied Lyapunov exponent to investigate the auto-parametric instability of a cable-stayed-beam system under deterministic and stochastic excitations. The Lyapunov exponent can be used to determine the stability of auto-parametric vibrations. The motion equation Eq. (20) of the structural system can be rewritten as the following differential equations with variable coefficients

$$\dot{\mathbf{z}}(t) = \boldsymbol{\psi}(t)\mathbf{z}(t) + \mathbf{q}(t) \quad (35)$$

where

$$\begin{cases} \mathbf{z}(t) = \left[\mathbf{a}(t), \dot{\mathbf{a}}(t)\right]^T \\ \boldsymbol{\psi}(t) = \begin{bmatrix} \mathbf{0} & \mathbf{I} \\ -\mathbf{M}^{-1}(\mathbf{K} - \mathbf{K}_G(t)) & -\mathbf{M}^{-1}\mathbf{C} \end{bmatrix} \\ \mathbf{q}(t) = \left[\mathbf{0}, \mathbf{M}^{-1}\mathbf{p}(t)\right]^T \end{cases} \quad (36)$$

According to Kr$\ddot{\mathbf{a}}$tzig *et al*. (1996), and Xia and Fujino (2006), the Lyapunov exponent of Eq. (35) can be defined as

$$\lambda_{LE(j)} = \lim_{t\to\infty}\frac{1}{t}\ln\frac{\left\|\mathbf{z}_j(t)\right\|}{\left\|\mathbf{z}_j(0)\right\|} \quad (37)$$

where $\mathbf{z}_j(0)$ denotes the initial perturbation vector in the j^{th} direction of the phase space. For a structural system, the $\mathbf{z}_j(0)$ can be determined by the j^{th} modal vector of the structure. If the j^{th} modal frequency and vector are respectively ω_j and $\boldsymbol{\varphi}_j$, then $\mathbf{z}_j(0)$ can be taken as

$$\mathbf{z}_j(0) = \left[\mathbf{a}_j(0), \dot{\mathbf{a}}_j(0)\right]^T = \left[k\boldsymbol{\varphi}_j, \mathbf{0}\right]^T \quad (j = 1,2,3,...,N) \quad (38)$$

where k is a constant, which ensures the initial perturbation to be a small value. For a specific excitation, we can obtain N Lyapunov exponents, i.e., $\lambda_{LE(j)}$ (j=1,2,3,..,N). Ordering them from largest to smallest, the stability of structural system can be determined by the largest Lyapunov exponent $\lambda_{LE(j)}$, i.e.

$$\begin{cases} \lambda_{LE(1)} < 0 & \textit{stability} \\ \lambda_{LE(1)} = 0 & \textit{stability boundary} \\ \lambda_{LE(1)} > 0 & \textit{instability} \end{cases} \quad (39)$$

3.3.2 The finite-time Lyapunov exponent

When Eq. (37) is applied to extract the Lyapunov exponent from an auto-parametric vibration, it needs a very long computational time to acquire a convergence value. The Lyapunov exponent is originally used for describing the nonlinear behavior of the system motion (Wolf 1985), so the response amplitude might be very large. However the finite element motion equations of framed structures are established on the basis of the small-deformation assumption, i.e., the motion equations are linear. When the time is big enough, the structural response might exceed the linear range. Under this circumstance, the structural responses cannot be controlled by the linear equations any more, thus the response results are not correct any longer. Therefore it is inappropriate to calculate the Lyapunov exponent by using Eq. (37) for the stability analysis of linear motion.

It can be seen from a typical time-history response of function $\ln[\|\mathbf{z}_j(t)\|/\|\mathbf{z}_j(0)\|]$ (see Fig. 3) that the response is also a backbone curve superimposed on a periodic perturbation. The backbone curve shows an interval of the initial transient disturbance in the initial period of time

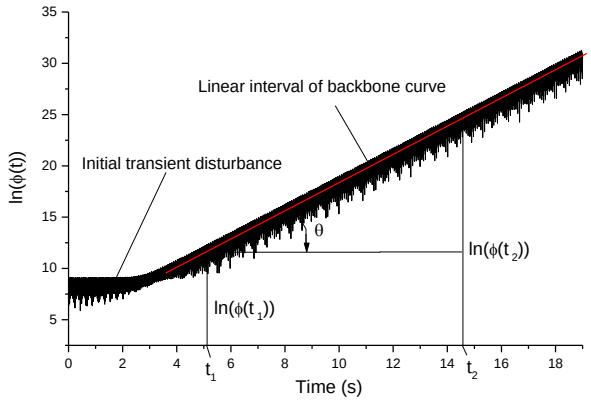

Fig. 3 A typical curve of function (ln[$\phi(t)$]=[$\|\mathbf{z}_j(t)\|/\|\mathbf{z}_j(0)\|$])

($0\le t\le t_1$), and a linear growth after the time $t_1(t_1<t<t_2)$, during which the response amplitude of the structural system is still within the linear limitation. So the average slope of backbone curve in the linear interval can be taken as a finite-time Lyapunov exponent $\lambda_{FLE(j)}$ to replace the Lyapunov exponent by Eq. (37), i.e.

$$\lambda_{FLE(j)}=\frac{1}{t_2-t_1}\left[\ln\frac{\|\mathbf{z}_j(t_2)\|}{\|\mathbf{z}_j(0)\|}-\ln\frac{\|\mathbf{z}_j(t_1)\|}{\|\mathbf{z}_j(0)\|}\right]=\frac{1}{t_2-t_1}\ln\frac{\|\mathbf{z}_j(t_2)\|}{\|\mathbf{z}_j(t_1)\|} \quad (40)$$

The finite-time Lyapunov exponents similar to Eq. (40) have been widely applied for dynamic stability analyses of different systems in other disciplines such as physics (Rosenstein *et al*. 1992), biomechanical engineering (Dingwell *et al*. 2001), electrical engineering (Elfrgani 2015), etc. The advantages of the finite-time Lyapunov exponent are that the calculated results are reliable, the influences of initial disturbances are removed, and the obtained instability boundaries are smooth.

The present numerical results show that the two methods by using EGE and the finite-time Lyapunov exponent can provide the same instability boundaries. However, the energy function ln[$E(t)/E_0$] has a clearer backbone line with a smaller perturbation than the function ln[$\|\mathbf{z}_j(t)\|/\|\mathbf{z}_j(0)\|$] (see Figs. 2 and 3). The EGE/EGC method is clearer as far as the physical interpretation is concerned.

4. Numerical examples

4.1 Parametric and auto-parametric resonances of a Γ-shaped frame

Fig. 4 shows a Γ-shaped frame which is subjected to a periodic load $P(t)=P_d\cos\omega t$. In this illustration, the lengths of beam-1 and beam-2 are both 6.0(m), the height and width of the beams' section are 0.08 (m) and 0.1 (m), respectively. The two beams are connected with a hinge joint, and the other ends of the two beams are clamped. The structure is made of steel, of which the mass density is ρ=7850 (kg/m^3), Young's modulus $E=2.0\times10^{11}$(N/m^2). The structural damping is not considered. The beam-1 and -2 are respectively discretized into two equal-length beam elements. Through a modal analysis, the fundamental

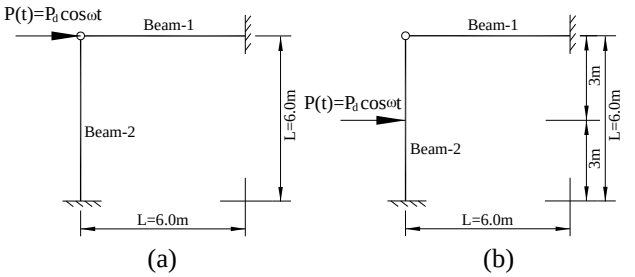

Fig. 4 A Γ-shaped frame subjected to a periodic load

(bending mode) frequencies of beam-1 and beam-2 can be respectively obtained, i.e., $\omega_1=\omega_2$=50.375(rad/s). When a horizontal static load acts on the joint, as shown in Fig.4(a), the corresponding static elastic buckling load of beam-1 can be calculated, i.e., $P_{cr}=4.909\times10^5$(N). In this example, the parametric resonance and auto-parametric resonance of the beam-1 in the first mode shape are respectively investigated.

4.1.1 Principal parametric resonance and stability boundaries

Consider the case, as shown in Fig. 4(a), where an external periodic load acts on the joint of beam-1 and -2. The periodic load can lead to a principal parametric resonance of beam-1. This problem can be solved in two different ways.

The first way is to establish and solve the global finite element equation (Eq. (20)), and to calculate the EGC of beam-1. Because this problem only involves the local instability of beam-1, the energy of beam-1 and its EGC are only considered here. The numerical EGC results of beam-1 are calculated and plotted in Fig. 5 (see the open circles). The principal stability boundary of beam-1 is obtained by the zero points of numerical EGC, as shown in Fig. 6 (see the solid line). Since the beam-1 can be equivalently regarded as a single-span beam that is clamped in one end and simply-supported in other end, the parametric resonance of the beam-1 in mode 1 is governed by the following Mathieu equation (Bolotin 1964, Xie 2006)

$$\ddot{q}_1(t)+\omega_1^2\left[1+\mu\cos\omega t\right]q_1(t)=0 \quad (41)$$

where $q_1(t)$ and $\ddot{q}_1(t)$ are the 1th generalized coordinate and its acceleration, respectively, ω_1 is the first modal frequency of the system, $\mu=P_d/P_{cr}$ the exciting coefficient, ω the excitation frequency. According to Li *et al*. (2016), the EGC of the parametrically excited systems that are governed by Mathieu equation (41) can be expressed as an analytical formula, i.e., EGC of beam-1 in mode 1 can be expressed as

$$\eta_1=\frac{\mu}{2}\sqrt{1-\left[\frac{r_1-2+\mu^2/32}{\mu/2}\right]^2} \qquad (\mu\le0.4) \quad (42)$$

where $r_1=\omega/\omega_1$ is the frequency ratio. The EGC curves of beam-1 can also be computed with Eq. (42). It can be seen from Fig. 5 that the numerical EGC results agree well with those by Eq. (42). The present EGC curves (semi-circles) are identical to the EGC curves (Li *et al*. 2016) of the other

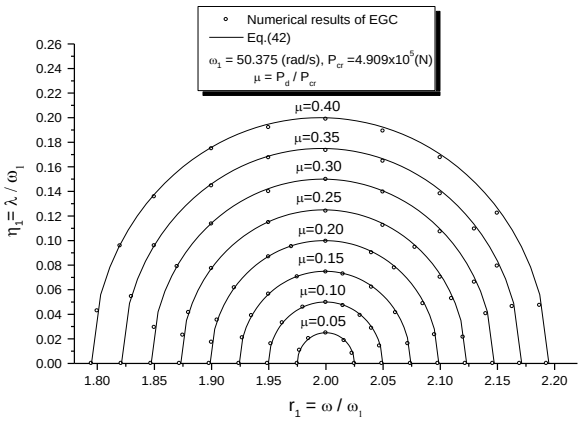

Fig. 5 Numerical and analytical EGC results of beam-1

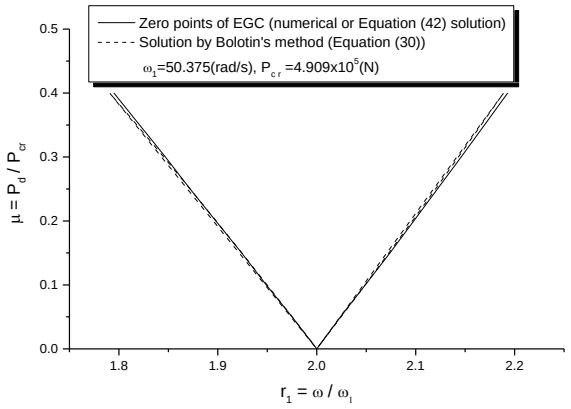

Fig. 6 Principal instability boundaries of beam-1

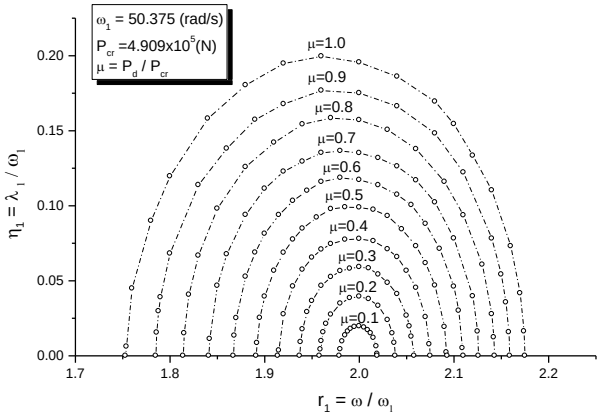

Fig. 7 The EGC results of beam-1

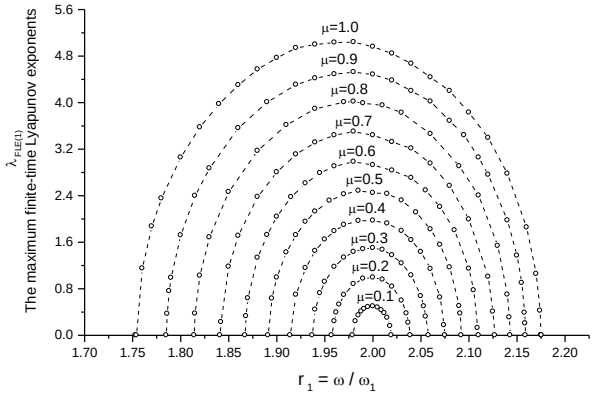

Fig. 8 The maximum finite-time Lyapunov exponents of beam-1

parametrically excited systems (such as contained fluid, simple pendulum etc.), which are governed by Mathieu equation. The principal instability boundary of beam-1 can also be determined by the zero points of Eq. (42) (η_1=0), as shown in Fig. 6 (see the solid line).

The second way is to establish the finite element equation Eq. (29), and to use Bolotin's method (Eq. (30)) for solving the principal instability boundary. The result is shown in Fig. 6 (see the dash line). It can be seen from Fig. 6 that the two boundary curves by EGC and Eq. (30) match well with each other.

4.1.2 Auto-parametric resonance and stability boundaries

When the external load acts on the center of beam-2, as shown in Fig. 4(b), the framed structure becomes an auto-parametric system. The beam-2 is the primary system, which can be regarded as a linear forced vibration system. The beam-1 is the secondary system, which is parametrically excited by the motion of beam-2. The geometric stiffness matrix of the beam-1 is periodically changed by the load from beam-2. In the finite element motion equation of beam-1, the coupling exists in the form of nonlinear product term $\mathbf{K}_{G1}(t)\mathbf{a}_1(t)$ (where $\mathbf{K}_{G1}(t)$ and $\mathbf{a}_1(t)$ are respectively the geometric stiffness matrix and nodal displacement vector of beam-1), in which $\mathbf{K}_{G1}(t)$ implicitly depends on the motion of beam-2 (or the load

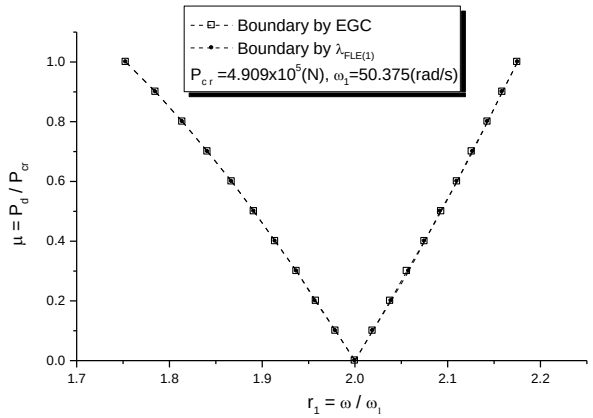

Fig. 9 Auto-parametric instability boundaries of beam-1

from beam-2). Therefore the secondary system (beam-2) is nonlinearly coupled by the primary system (beam-1).

A periodic axial load is transmitted from the primary system (beam-2) into the second system (beam-1) through the hinge joint. This transmitted axial load may result in an auto-parametric instability of beam-1. The global motion equation of the structure appears in a non-homogeneous Mathieu-Hill equation (Eq. (20)). The numerical EGC and the finite-time Lyapunov exponent of beam-1 are respectively calculated to determine the stability boundary of beam-1. Figs. 7 and 8 respectively show the distribution

curves of EGC and the maximum finite-time Lyapunov exponent for beam-1, which vibrates in the first mode. It is easily found from Fig. 7 that the EGC curves are not the semi circles (see Fig. 5) any more. That is because the auto-parametric instability of beam-1 is affected by beam-2. On the basis of the zero points of EGC and the Lyapunov exponent, the auto-parametric instability boundaries of beam-1 are easily obtained as shown in Fig. 9. It can be seen that the two instability boundaries by EGC and the maximum finite-time Lyapunov exponent ($\lambda_{FLE(1)}$) agree accurately.

4.1.3 The effect of relative stiffness between the primary and secondary systems on auto-parametric instability boundaries

Take the frame in Fig. 4(b) as this example, when the relative stiffness of primary system (beam-2) and secondary system (beam-1) changes, the auto-parametric instability boundary of beam-1 will vary accordingly. For simplicity, the variation of Young's modulus of beam-2 is only considered. The Young's modulus of beam-2 is chosen as E_2=(200~3200)(GP_a), and the rest of the computing data remain unchanged. The changes of relative stiffness can be represented by the first natural frequency ratios of beam-2 and beam-1, which are listed in Table 1.

For the various frequency ratios, the auto-parametric instability boundaries of beam-1 are calculated as shown in Fig. 10. It can be seen that the instability boundaries vary greatly with the variation of the frequency ratio.

4.1.4 Auto-parametric resonance induced by a normal resonance (Γ -shaped frame)

Consider the example of Sect. 4.1.3. When the frequency ratio ω_2/ω_1 equals 2 (i.e., the relative stiffness ratio E_2/E_1 is 4), and the forcing frequency and amplitude are respectively $\omega=\omega_2=2\omega_1$ and $P_d=4.91\times10^3$ (N), then the external periodic force $P_d\times\cos\omega t$ can arouse the normal resonance of beam-2. Meanwhile, the auto-parametric resonance of beam-1 will be induced by this normal resonance. Figs. 11 and 12 respectively show the normal resonance response of beam-2 and auto-parametric resonance response of beam-1. It can be seen that the center-point displacement amplitude of beam-2 increases with time linearly, but the center-point displacement amplitude of beam-1 increases exponentially. The EGE and finite-time Lyapunov exponent (FLE) of beam-1 are no longer the constants, but increase with time. Because the response of secondary system increases sharply, the consequence of the auto-parametric resonance might be disastrous. From this typical example, it can be found that the effect of internal axial force of beam-1 is amplified during the load transmission. The risk of auto-parametric resonance of the framed structure is greatly enlarged. This auto-parametric resonance of secondary system induced by a normal resonance of primary system can be called as "auto-parametric internal resonance".

In the view of bridge engineering, this example implies that a small periodic load acting on the bridge pier, for instance the vortex-induced force by river, might cause a strong auto-parametric resonance of the bridge girder.

If the structural damping is considered, the damping matrix of the Γ-shaped frame in Fig. 4 can be assumed as a stiffness-proportional damping one (Chopra 2007)

$$\mathbf{C} = \beta_k \cdot \mathbf{K} \tag{43}$$

Table 1 The first natural frequency ratios of beam-2 and -1

E_2 (GP_a)	200	312.5	1512.5	1800	3200
ω_2/ω_1	1.0	1.25	2.75	3.0	4.0

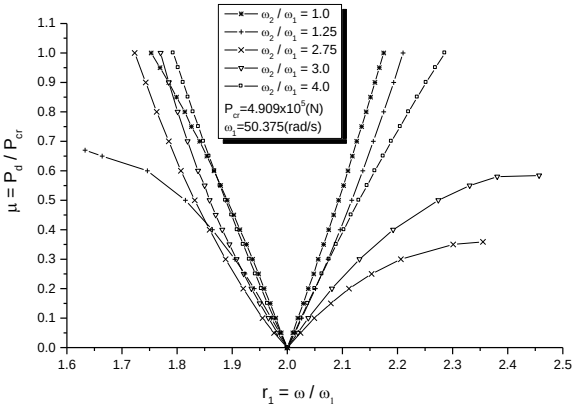

Fig. 10 Variations of auto-parametric instability boundaries of beam-1 with the relative frequency ratios (without damping)

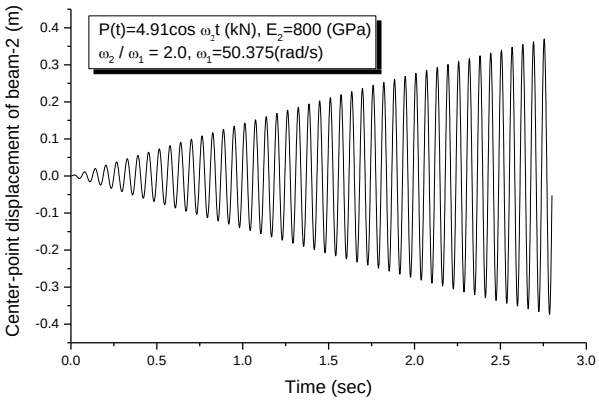

Fig. 11 Normal resonance response of beam-2

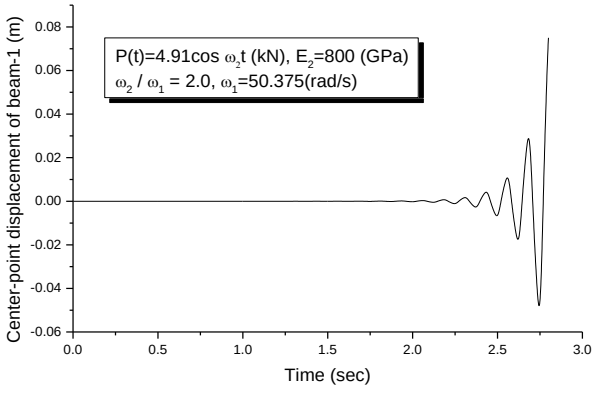

Fig. 12 Auto-parametric resonance response of beam-1

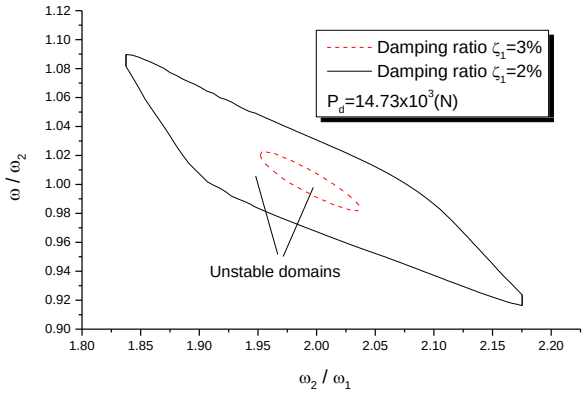

Fig. 13 Instability boundaries of auto-parametric resonance of beam-1 near ω_2/ω_1=2.0

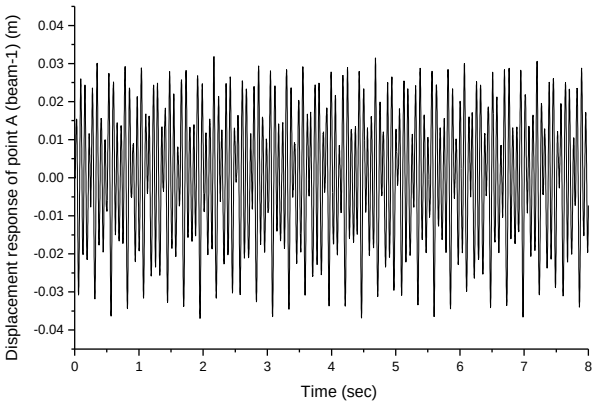

Fig. 15 Bounded forced response of point A (beam-1)

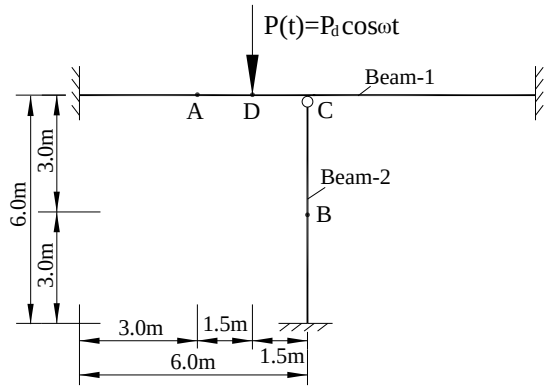

Fig. 14 A T-shaped frame subjected to a periodic load

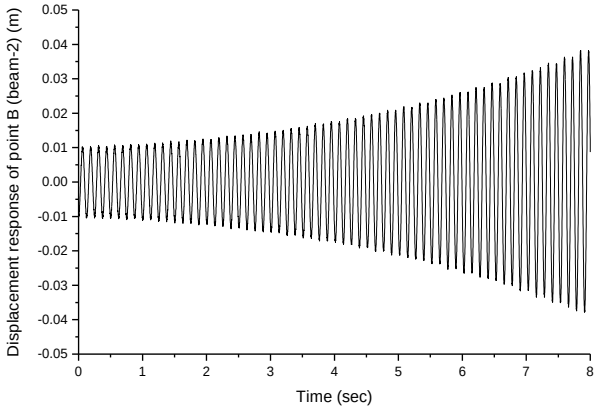

Fig. 16 Auto-parametric resonance response of point B (beam-2)

where β_k is a constant. Because the auto-parametric resonance response of beam-1 is focused on in this example, the coefficient β_k can be given by

$$\beta_k = \frac{2\zeta_1}{\omega_1} \tag{44}$$

where ω_1 and ζ_1 are respectively the first frequency and damping ratio of beam-1. When the frequency ratio ω_2/ω_1 is near 2, and the exciting frequency ω is close to ω_2, the "auto-parametric internal resonance" will occur. The structural damping will make the unstable domain smaller. Fig. 13 shows the instability boundary of auto-parametric resonance of beam-1 near ω_2/ω_1=2.0, in which the forcing amplitude P_d=14.73×10^3 (N). It can be seen that the larger the damping ratio is, the smaller the unstable domain is. When the damping ratio is approximately 3.085%, the unstable domain tends to a point, i.e., the unstable domain disappears. It is indicated that the critical damping ratio of this example is $\zeta_{1cr}\approx$3.085%. The similar results can be obtained for the other different exciting amplitudes.

4.2 Auto-parametric resonances analyses for a T-shaped frame

4.2.1 Auto-parametric resonance by an external periodic load

Fig. 14 shows a T-shaped frame, in which the two ends of beam-1 are clamped, the mid-point of beam-1 is connected with one end of beam-2 with a hinge, and the other end of beam-2 is clamped. The lengths of the beam-1 and beam-2 are respectively 12.0 (m) and 6.0 (m). The height and width of the beams' section are respectively 0.08 (m) and 0.1 (m). The mass density and Young's modulus of the frame material are 7850 (kg/m^3) and 2.0×10^{11} (N/m^2), respectively. The structural damping is not considered. The beam-1 and -2 are respectively discretized into eight and four equal-length beam elements. Through a modal analysis, the fundamental frequencies of beam-1 and -2 are respectively calculated, i.e., $\omega_1=\omega_2$ = 49.940 (rad/s). When a static vertical force exerts on the joint C, the corresponding elastic buckling load of beam-2 is calculated as P_{cr}=4.77×10^5 (N). The beam-1 is exerted to an external periodic load $P(t)=P_d\cos\omega t$ at point D. The amplitude and frequency of the periodic load are assumed as P_d =0.05P_{cr} and ω =2ω_1=99.861 (rad/s). In this framed structure, beam-1 is the primary system and beam-2 is the second system. As is the case in Fig. 4(b), the secondary system is nonlinearly coupled by the primary system. The external periodic load $P(t)$ acting on the primary system can give rise to the auto-parametric resonance of the second system. Figs. 15 and 16 respectively show the time-history responses of point A (in beam-1) and point B (in beam-2). It can be seen that the beam-1 experiences a bounded forced oscillation, while the beam-2 undergoes an auto-parametric resonance.

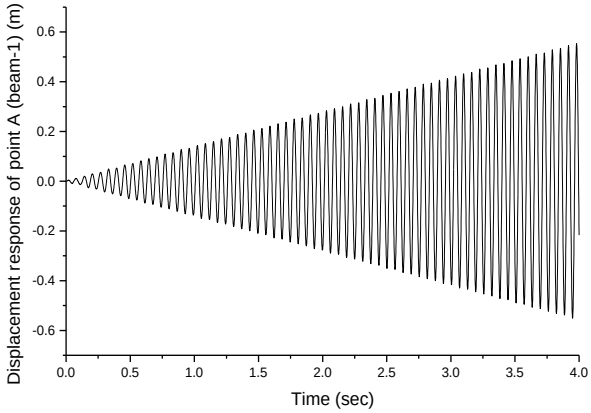

Fig. 17 Forced (normal) resonance response of point A (beam-1)

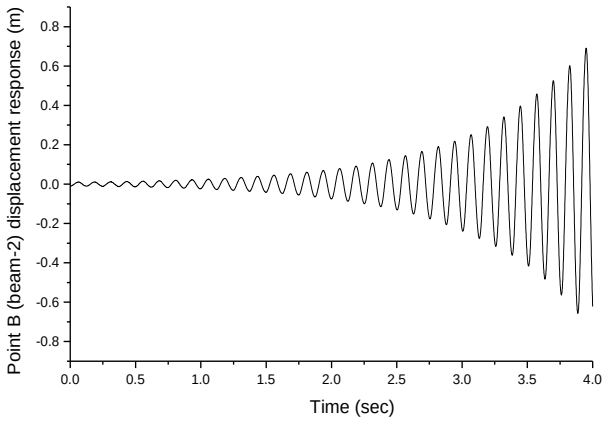

Fig. 18 Auto-parametric resonance response of point B (beam-2)

4.2.2 Auto-parametric resonance induced by a normal resonance

The T-shaped frame is same as in Fig. 14, in which the height of the beam-1 section is changed as 0.16 (m), and the rest of the parameters remain unchanged. Therefore the fundamental frequencies of beam-1 and -2 are respectively calculated as ω_1=99.861 (rad/s) and ω_2=49.940 (rad/s). When the amplitude and frequency of the periodic load $P(t)$ are assumed as P_d=0.05P_{cr} and ω=ω_1=2ω_2=99.861 (rad/s), the beam-1 experiences a forced (normal) resonance as shown in Fig. 17, while the beam-2 undergoes an auto-parametric resonance as shown in Fig. 18. Comparing the response curves in Figs. 16 and 18, it can be found that the growth rate of displacement in Fig. 18 is much greater than that in Fig. 16. It is indicated that the "auto-parametric internal resonance" (the auto-parametric resonance induced by a normal resonance) is much more dangerous.

In the view of bridge engineering, this example implies that the small periodic load acting on the bridge girder, such as a cyclical load by the running vehicle, might give rise to a strong auto-parametric resonance of the bridge pier.

The instability boundaries near the "auto-parametric internal resonance" are similar to those of the above Γ-shaped frame (Sect. 4.1.4.).

5. Experimental verification for the auto-parametric instability boundaries

An auto-parametric resonance test of a framed structure is conducted to observe the actual dynamic instability phenomenon of the structure, and to verify the theoretical predictions.

5.1 Test devices and model

The test devices used for present experimental study are respectively shown in Figs. 19 and 20. The test model is a Γ-shaped frame, which is composed of a horizontal beam (beam-1) and a vertical beam (beam-2). The beam-1 and beam-2 is connected with a hinge joint, and the other ends of the two beams are clamped on the supports. The test beams are made of stainless steel. The geometric dimensions of the test model are illustrated in Fig. 21.

As illustrated in Fig. 19, a perfect sinusoidal signal is generated by the signal generator (SPF05A), then amplified by the power amplifier (HEA-50), and finally transmitted to the vibrationexciter (HEV-50). This vibrationexciter can exert a horizontal sinusoidal displacement excitation on the beam-2. The position of forcing point is shown in Fig. 21. One laser displacement sensor (SUNX-ANR 1215) is used to measure the displacement of the forcing point, which can be regarded as a displacement excitation from the vibration exciter. The other laser sensor is employed to measure the (unstable) displacement response of middle point of beam-1. The two laser signals are simultaneously collected by the data acquisition instrument (INV306U-A), and analyzed by the signal analyzer (INV306U), then recorded and displayed by the computer.

A typical measured displacement excitation acting on the beam-2 is displayed in Fig. 22, from which the amplitude and frequency of the excitation can be determined. A typical instability displacement response of beam-1 is measured as shown in Fig. 23, from which the response frequency can be easily obtained by using FFT.

By means of a free vibration test, we can obtain the free-decay curve of displacement of beam-1, as shown in Fig. 24. The damping ratio ζ of beam-1 can be computed by the following expression

Table 2 Measured and calculated data of the test model-1 (case 1)

	Dimensions $b\times h$ (mm^2)	Measured fundamental frequency (rad/s)	Calculated fundamental frequency (rad/s)	Measured damping ratio
Beam-1	37.6×0.58	40.84	41.49	0.55%
Beam-2	37×0.9	284.70	285.70	

Table 3 Measured and calculated data of the test model-2 (case 2)

	Dimensions $b\times h$ (mm^2)	Measured fundamental frequency (rad/s)	Calculated fundamental frequency (rad/s)	Measured damping ratio
Beam-1	37.6×0.58	39.40	41.49	0.55%
Beam-2	37×0.7	218.91	222.24	

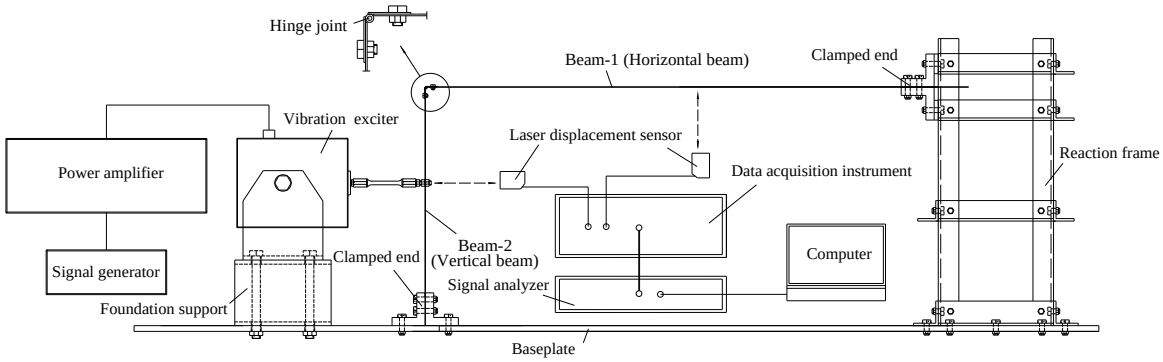

Fig. 19 Experimental schematic diagram

Fig. 20 Photo of experimental facilities

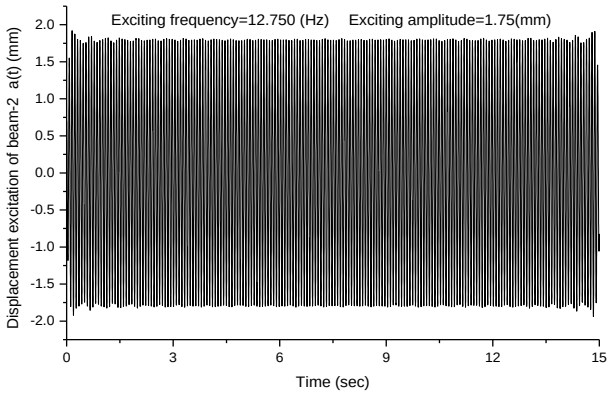

Fig. 22 A typical measured displacement excitation acting on the beam-2

$$\zeta = \frac{1}{2\pi N}\ln\left(\frac{h_1}{h_{N+1}}\right) \tag{45}$$

where h_1 and h_{N+1} are respectively the displacement amplitudes in 1 and N+1 cycles of oscillation.

There are two test cases in this experiment. The measured and calculated data of the test models for the two cases are respectively obtained in Tables 2 and 3. The theoretical (calculated) frequencies are extracted by the modal analysis method.

5.2 Theoretical instability boundaries

The framed structure is discretized into four elements with nodes 1~5 as shown in Fig. 21. A known horizontal

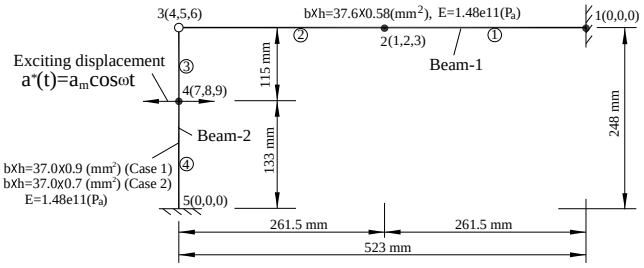

Fig. 21 Calculating diagram of test model

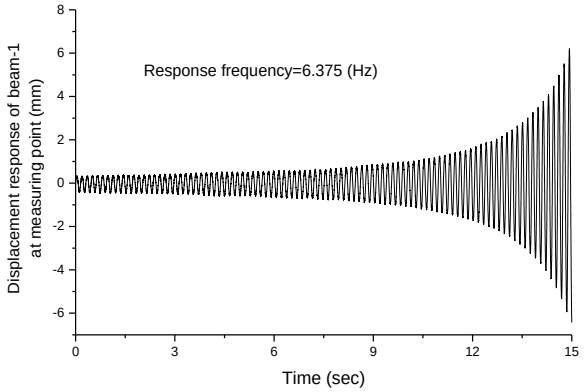

Fig. 23 A typical measured unstable response of beam-1

displacement excitation $a^*(t) = a_m \cos \omega t$ (the corresponding velocity and acceleration are respectively $\dot{a}^*(t) = -a_m \sin \omega t$ and $\ddot{a}^*(t) = -a_m \omega^2 \cos \omega t$) is applied to node 4. The mass and stiffness matrices (including geometric stiffness matrix) of the test model are all (9×9) matrices, the nodal acceleration, velocity and displacement vectors are all (9×1) vectors, and external load vector is $\mathbf{p}^T(t) = (0,0,0,0,0,0,p(t),0,0)$, in which $\mathbf{p}(t)$ is the unknown horizontal force acting at node 4. The damping matrix of the test model is established by Eqs. (43) and (44). The ω_1 and ζ_1 in Eq. (44), which are respectively the first computed frequency and measured damping ratio of beam-1, can be obtained from Tables 2 and 3.

In order to apply the computational formulation of Section 2.4, we need to turn the format of present global finite element equation into that of Eq. (26). We first exchange columns 7 and 9 of the mass, damping and stiffness matrices, and exchanges rows 7 and 9 of these

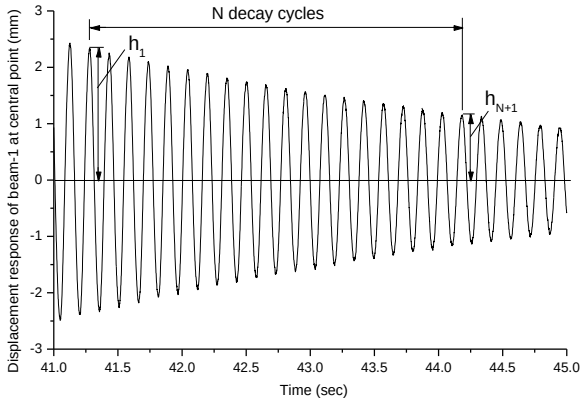

Fig. 24 The free-decay curve of displacement of beam-1

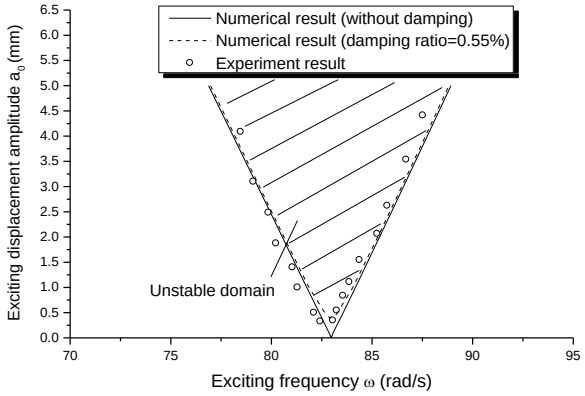

Fig. 26 Auto-parametric instability boundaries of beam-1 (Case 2)

matrices, then exchanges rows 7 and 9 of load vector $\mathbf{p}(t)$, therefore the load vector becomes $\mathbf{p}^T(t)=(0,0,0,0,0,0,0,0,p(t))$.

After the above operation, the displacements corresponding to the DOF (degree of freedom) 9 and DOF 7 respectively represent the horizontal and rotation displacements of node 4, i.e., the known forcing displacement, velocity and acceleration are respectively $a_9(t)=a_m\cos\omega t$, $\dot{a}_9(t)=-a_m\omega\sin\omega t$ and $\ddot{a}_9(t)=-a_m\omega^2\cos\omega t$, while the corresponding force p_9=$p(t)$ is unknown. Therefore the format of modified finite element equation is same as Eq. (27), which can be solved by the calculating scheme of Sect. 2.3. Then the time-history responses of beam-1 can be obtained. Based on the above EGE (or FLE) method in Section 3, the theoretical instability boundaries of beam-1 are calculated as shown in Figs.25 and 26 (see the solid and dash lines).

5.3 Experimental instability boundaries

The experimental values of instability boundaries of beam-1 are carefully found by fixing the excitation amplitude and varying the excitation frequency in the vicinity of the theoretically predicted boundaries until the unstable motion began to appear or disappear on the computer screen. Figs. 25 and 26 respectively show the auto-parametric instability boundaries of beam-1 for cases 1 and 2. It can be seen that the experimental values (see the

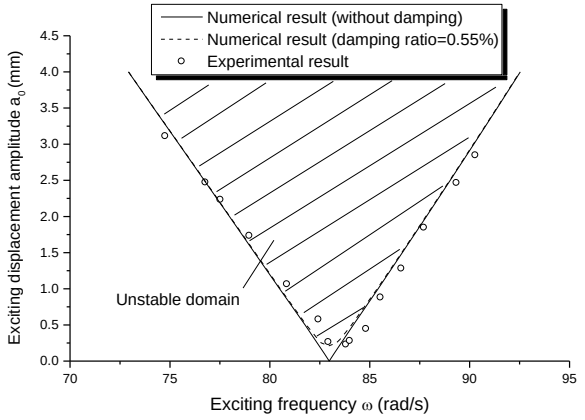

Fig. 25 Auto-parametric instability boundaries of beam-1 (Case 1)

open circles) have a good agreement with the numerical solutions. From Figs. 25 and 26, it can also be found that the unstable domains decrease a little due to the small structural damping. The damping effect on the instability boundaries can be well modeled by the linear damping ratio.

5.4 Verification of the semi-trivial solution

The above theoretical and experimental results have shown that there are two kinds of solutions in the system. For a displacement excitation $a^*(t)=a_m\cos\omega t$, when the exciting parameters (a_m,ω) fall inside the unstable domain, the solution is unstable, which we call auto-parametric resonance. The typical displacement solutions of the primary and secondary systems are respectively shown in Figs. 22 and 23. When the exciting parameters (a_m,ω) fall outside the unstable domain, the solution is stable. The displacement solution of beam-2 (the primary system) is similar to the solution in Fig. 22, while the displacement response of beam-1 (the second system) is zero (motionless). This kind of solution is called the semi-trivial solution (Tondl *et al*. (2000)).

6. Conclusions

In this paper, the finite element equations of motion were established for the framed structures subjected to the periodic loads. The numerical methods were developed for solving the auto-parametric resonance responses and instability boundaries. Some numerical examples were presented. An auto-parametric resonance experiment of a framed structure was conducted for verifying the theoretical predictions. The conclusions of this research are as follows.

(1) A framed structure may be composed of two sub-structures, which are linked by a hinged joint. One sub-structure is the primary system and the other is the secondary system. The primary system, which is subjected to the periodic external excitation, can give rise to an auto-parametric resonance of the second system. The auto-

parametric resonance originates from the geometric-stiffness matrix effect that is produced by the internal axial force. When the element geometric-stiffness matrix is considered, the motion equations of framed structures can be generally expressed as the non-homogeneous Mathieu-Hill equations. The time-history responses of the non-homogeneous Mathieu-Hill equations can be solved by the Newmark's method.

(2) Both EGE/EGC and FLE can be employed for determining the auto-parametric instability boundaries. The two methods can give the same instability-boundary results.

(3) The numerical results show that the changes of relative stiffness between the primary and secondary systems have an important effect on the auto-parametric instability boundaries of the second system. The auto-parametric resonance of the second system can be induced by a normal resonance of the primary system, which is called the "auto-parametric internal resonance". The internal axial force of a beam element of the secondary system may be amplified during the process of the load-transmission, consequently, the risk of auto-parametric resonance is greatly enlarged.

(4) The experimental results of auto-parametric instability boundaries are accord with the numerical solutions. It indicates that the present calculation method is valid and effective.

Acknowledgments

This study was supported by the National Science Foundation of China (Grant No. 51279133). The authors gratefully acknowledge this financial support.

References

Basar, Y., Eller, C. and Kratzig, W.B. (1987), "Finite element procedures for parametric resonance phenomena of arbitrary elastic shell structures", *Comput. Mech.*, **2**, 89-98.

Bathe, K.J. (1996), *Finite Element Procedures*, Prentice Hall, New Jersey.

Bolotin, V.V. (1964), *The dynamic stability of elastic systems*, Holden Day, San Francisco.

Briseghella, L., Majorana, C.E. and Pellegrino, C. (1998), "Dynamic stability of elastic structures: a finite element approach", *Comput. Struct.*, **69**, 11-25.

Chopra, A.K. (2007), *Dynamics of Structures: Theory and Applications to Earthquake Engineering*, Prentice Hall, New Jersey.

Clough, R.W. and Penzien J. (2003), *Dynamics of Structures*, Third Edition, Computers & Structures, Inc., Berkeley.

Dingwell, J.B., Cusumano, J.P., Cavanagh, P.R. and Sternad, D. (2001), "Local dynamic stability versus kinematic variability of continuous overground and treadmill walking", *J. Biomech. Eng.*, **123**, 27-32.

Elfrgani, A.M., Moussounda, R. and Rojas, R.G. (2015), "Stability assessment of non-Foster circuits based on time-domain method", *IET Microw. Anten. Propagat.*, **9**(15), 1769-1777.

Kr ä tzig, W. B., Bsar, Y., and Nawrotzki, P. (1996), "Dynamic structural instabilities", *Dynamics of Civil Engineering Structures*, Eds. W.B. Kr ä tzig, Y. Bsar and P. Nawrotzki, Balkema, Rotterdam.

Kumar, R., Kumar, A. and Panda, S.K. (2015), "Parametric Resonance of composite skew plate under non-uniform in-plane loading", *Struct. Eng. Mech.*, **55**(2), 435-459.

Li, Y. and Wang, Z. (2016), "Unstable characteristics of two-dimensional parametric sloshing in various shape tanks: theoretical and experimental analyses", *J. Vib. Control*, **22**(19), 4025-4046.

Li, Y., Wang, L. and Yu, Y. (2016), "Stability analysis of parametrically excited systems using the energy-growth exponent/coefficient", *Int. J. Struct. Stab. Dyn.*, **16**(10), 1750018.

Majorana, C.E. and Pellegrino, C.D. (1997), "Dynamic stability of elastically constrained beams: an exact approach", *Eng. Comput.*, **14**(7), 792-805.

Majorana, C.E. and Pomaro, B. (2011), "Dynamic stability of an elastic beam with visco-elastic translational and rotational supports", *Eng. Comput.*, **28**(2), 114-129.

Majorana, C.E. and Pomaro, B. (2012), "Dynamic stability of an elastic beam with visco-elasto-damaged translational and rotational supports", *J. Eng. Mech.*, **138**(6), 582-590.

Mishra, U.K. and Sahu, S.K. (2015), "Parametric instability of beams with transverse cracks subjected to harmonic in-plane loading", *Int. J. Struct. Stab. Dyn.*, **15**(1), 1540006.

Náprstek, J. and Fischer, C. (2015), "Dynamic stability of a vertically excited non-linear continuous system", *Comput. Struct.*, **155**, 106-114.

Pradyumna, S. and Gupta, A. (2011), "Dynamic stability of laminated composite plates with piezoelectric layers subjected to periodic in-plane load", *Int. J. Struct. Stab. Dyn.*, **11**(2), 297-311.

Rosenstein, M.T., Collins, J.J. and Luca, C.J.D. (1993), "A practical method for calculating largest Lyapunov exponents from small data sets", *Physica D: Nonlin. Phenomena*, **65**(1-2), 117-134.

Shastry, B.P. and Rao, G.V. (1984), "Dynamic stability of bars considering shear deformation and rotatory inertia", *Comput. Struct.*, **19**, 823-7.

Shastry, B.P. and Rao, G.V. (1986), "Dynamic stability of a short cantilever column subjected to distributed axial loads", *Comput. Struct.*, **22**, 1063-1064.

Tondl, A., Ruijgrok, M., Verhulst, F. and Nabergoj, R. (2000), *Autoparametric Resonance in Mechanical Systems*, Cambridge University Press, Cambridge.

Wang, X. (2003), *Finite Element Method*, Tsinghua University Press, Beijing. (in Chinese)

Xia, Y. and Fujino, Y. (2006), "Auto-parametric vibration of a cable-stayed-beam structure under random excitation", *J. Eng. Mech.*, **132**(3), 279-286.

Xie, W.C. (2006), *Dynamic Stability of Structures*, Cambridge University Press, New York.

Wolf, A., Swift, J.B., Swinney, H.L. and Vastano, J.A. (1985), "Determining Lyapunov exponents from a time series", *Physica D: Nonlin. Phenomena*, **16**, 285-317.

CC